Heterogeneous lasers and coupling to Si_3N_4 near 1060 nm

J. T. Bovington,* M. J. R. Heck, and J. E. Bowers

Department of Electrical & Computer Engineering, University of California Santa Barbara, California 93106, USA

**Corresponding author: jock@ece.ucsb.edu*

Received August 11, 2014; accepted August 30, 2014;
posted September 15, 2014 (Doc. ID 213511); published October 14, 2014

A III–V/Si_3N_4 platform on silicon is presented capable of broad-spectral performance with initial heterogeneous lasers near 1060 nm. Continuous wave Fabry–Perot laser results for heterogeneous InGaAs/GaAs multiple quantum well (MQW) laser with output power approaching 0.25 mW on Si is demonstrated. Taper transmission loss measurements from III–V to Si_3N_4 are measured to be 2.5 ± 0.75 dB. © 2014 Optical Society of America

OCIS codes: (140.2020) Diode lasers; (250.5300) Photonic integrated circuits.
http://dx.doi.org/10.1364/OL.39.006017

Traction has been made in recent years developing III–V/Si heterogeneous lasers using wafer bonding of unprocessed InP-based material to silicon-on-insulator (SOI) in order to leverage Si fabrication facilities, diagnostics, and process controls for III–V on Si processing [1,2]. The emergence of high-volume datacom products using this technology and interest in III–V on Si for electronics will open these facilities to other products, including using multi-project wafers with different band gap materials [3]. In this work, we utilize similar bonding and process methodology to enable integration of new components at shorter wavelengths, starting with an InGaAs/GaAsP MQW laser operating near 1060 nm. This wavelength is absorbed in silicon, so we use a SiO_2 clad Si_3N_4 waveguide coupled to III–V via tapers. Figure 1 shows our concept of a directly bonded III–V laser onto Si_3N_4 waveguides, processed post-bond for lithographic alignments and resolution in III–V device fabrication. This approach can be used at wavelengths from the visible to the infrared to integrate lasers and other active components to low-loss Si_3N_4 waveguides and devices such as arrayed waveguide gratings (AWGs).

Low water absorption near 1060 nm is great for applications in sensing, free space communications, medical applications, LiDAR, high-power low-divergence lasers [4], and seed sources to fiber lasers [5]. Integration at these wavelengths enable novel systems for high-power beam combining, mode converters for low-divergence beams, lithographically defined interferometric technologies such as balanced photo detection, and so much more. Utilizing Si_3N_4 passive waveguides is desirable for integrating devices across a broader spectral range than anything previously demonstrated [6] or for circuits requiring loss, less than 0.1 dB/m at 1.58 μm [7], or the order of magnitude lower thermal drift compared to Si. Finally, the cost of such circuits built on bulk Si can be lower than SOI-based designs if you do not need Si active components.

Figure 2 details the process flow for both the lasers and tapers. Note, that no Si_3N_4 waveguide is present under the Fabry–Perot lasers as the mode is confined by the III–V and oxidation aperture. Also, the tapered test structures do not have metallization or a p-mesa as the MQW material would absorb the transmission. 200 nm of LPCVD Si_3N_4 is deposited on thermally oxidized Si wafers, annealed at 900°C for 6 h and then patterned by ASML S500/300 DUV stepper and a $CHF_3:CF_4:O_2$ inductively coupled plasma dry etch. Patterned wafers are then clad with a PECVD SiO_2 partial upper cladding and chemically mechanically polished to achieve ∼0.5 nm RMS roughness. A gap from the Si_3N_4 waveguide to the bonding surface was 200 nm with a ±50 nm deviation. Vertical channels (VCs) were etched into the SiO_2 to improve bonding [8]. InGaAs/GaAs MQW laser material grown by metal-organic chemical vapor deposition is bonded to SiO_2 on Si following an O_2 plasma treatment and anneal at 300°C. The GaAs growth substrate is lapped to ∼100 μm and selectively spray etched using a $NH_4OH:H_2O_2$ (1:30) solution terminating on the 200-nm InGaP etch stop layer.

Laser p-mesas were then patterned and dry etched using a $Cl_2:N_2:H_2$ etch with a SiO_2 hardmask and stopped in the lower n-GaAs contact layer using a laser monitor. The VC mask was reused to open all VCs before an AlGaAs wet oxidation was performed at 365°C in a 50-mm Lindberg furnace with 10 sccm of N_2 carrier gas bubbled through an 80°C deionized wafer beaker. Without reopening the VCs, pressure in the covered VCs causes them to burst and redeposit III–V onto the sample. The oxidation aperture forms both a current guide and optical guide as shown in Fig. 3. Two additional tapers were formed by dry etching and selective wet etching to stop cleanly on the top of an InGaAs/GaAsP superlattice and the bonding surface. AuGe/Ni/Au (70/15/500 nm) n-metal was e-beam evaporated onto 2×10^{18} cm^{-1} n-GaAs and lifted-off, rapid annealed at

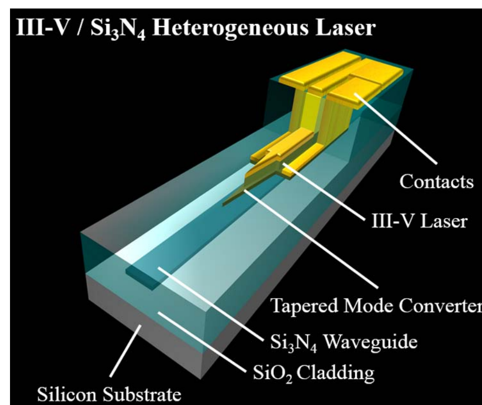

Fig. 1. Schematic of III–V/Si_3N_4 heterogeneous laser with III–V tapers coupling III–V to Si_3N_4

0146-9592/14/206017-04$15.00/0 © 2014 Optical Society of America

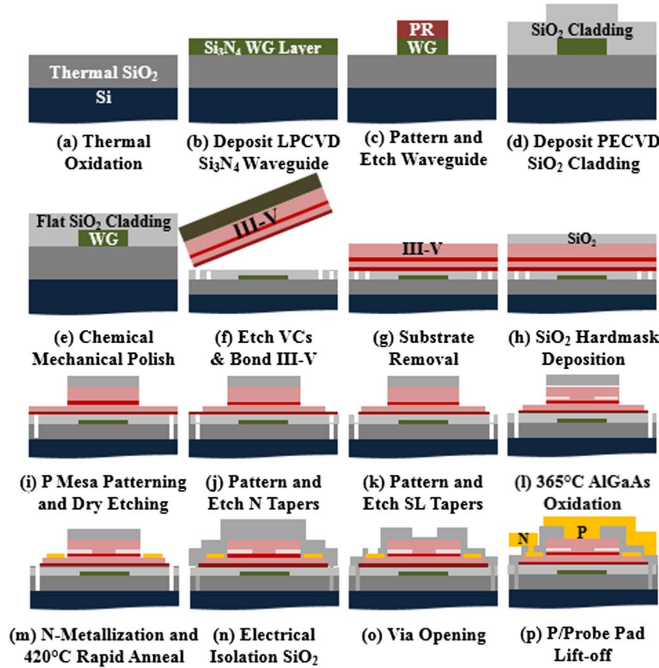

Fig. 2. Process for Fabry–Perot lasers and mode converters.

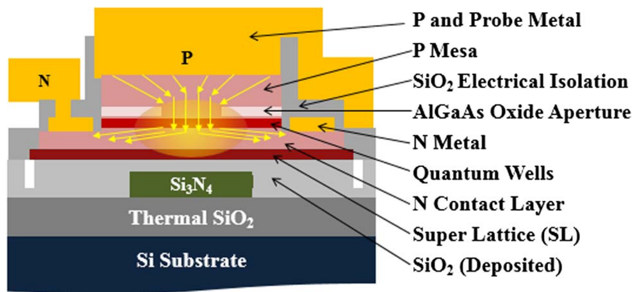

Fig. 3. Laser cross-section. In bulk of the gain region.

420°C for 30 s, then covered in a SiO_2 electrical isolation layer. Vias were made in the isolation and then a Ti/Pt/Au (5/30/1500 nm) e-beam evaporation was made to 1×10^{18} cm^{-1} p-GaAs and lifted off to form probe pads to the n contacts. Two experiments were done to prove the feasibility of integrating bonded III–V lasers with Si_3N_4 waveguides. First, we bonded and fabricated lasers on a thermal oxide layer. Laser data are presented in Section III. Second, we fabricated passive III–V to Si_3N_4 taper loss test structures by the full process shown in Fig. 2. These results are presented in Section IV.

Electrically pumped Fabry–Perot lasers were made by dicing III–V on SiO_2 on Si bars into different lengths, and polishing these to create facets. Multiple mesa widths were fabricated to vary the width of the current channel. All confinement factors in the quantum wells were simulated to be 0.09. The optimum p-mesa width of 12 μm with 4-μm-wide current apertures are presented below. Table 1 shows the layers of the MQW InGaAs/GaAsP epitaxial material prebonding.

Continuous-wave (CW) laser operation was observed at 12.3°C in a 2.4-mm-long laser whose optical power–current–voltage (LIV) curves are shown in Fig. 4. The high-diode turn on voltage is due to residual p-InGaP etch stop material above the p-GaAs contact.

Additionally, thermal impedance is higher in these designs than those on a native substrate owing to the 5 μm of lower SiO_2 cladding selected for better compatibility with thin Si_3N_4 cores for low loss [7].

The increase in active temperature is estimated to be ~34°C from the spectra in Fig. 4, assuming the material bandgap changes at a rate of 0.5 nm/K [9]. From this the thermal impedance is ~48.5°C/W for this 2.4-mm device. This is expectedly higher than that reported on InP type hybrid silicon lasers with 1-μm buried oxide [10], and in reasonable agreement with heat-transfer simulations of similar laser structures in COMSOL with 5-μm lower SiO_2 cladding. As a result of this self-heating, the threshold current was seen to increase from 100 to 163 mA for pulsed and CW. Flip-chip bonding to AlN or other high thermal conductivity electrical interconnection boards would improve the thermal performance.

Different length lasers were tested pulsed with 600-ns pulses at 1-kHz repetition rates at 20°C. Threshold currents below 20 mA for 600-μm-long lasers are shown in Fig. 5. The internal loss was calculated by cutback measurements for devices with 12-μm mesas and 4-μm-wide current apertures to be 6.2 cm^{-1}. The analysis used Eq. (1) and the curve fit to the best devices of each length in terms of inverse differential quantum efficiency, η_d, plotted in Fig. 6 [11].

Table 1. Laser Epitaxial Layer Stack

Function	Material	A1 (%)	t (nm)	Doping	Type
Bonding SL	InGaAs/GaAsP	—	72	2.7E + 18	n-Si
n-Contact	GaAs	—	200	2.7E + 18	n-Si
n-GRINSCH	AlGaAs	10 → 30	48	2.7E + 18	n-Si
Barrier	GaAs	—	10		UID
$(3x/2x)$ QW/Barriei	InGaAs/GaAsP	—	8/8		UID
Barrier	GaAs	—	10		UID
p-SCH	AlGaAs	30 → 80	88	7.5E + 17	p-C
AlO_x-aperture	AlGaAs	98	SO	7.5E + 17	p-C
p-Cladding	AlGaAs	80	1500	7.5E + 17	p-C
Grade	AlGaAs	80 → 10	200	7.5E + 17	p-C
p-Contact	GaAs	—	100	1.0E + 18	p-C
Etch stop	InGaP	—	200	1.0E + 18	p-C
Buffer	GaAs	—	500	1.0E + 18	p-C
Substrate	GaAs	—	625,000	>1E + 18	n-Si

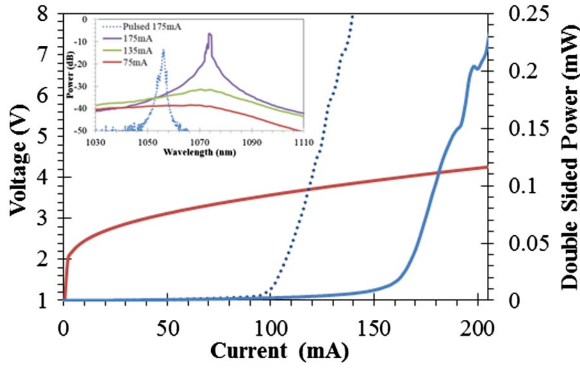

Fig. 4. LI curve (blue) and IV curve (red) of a 2.4-mm-long, 12-μm-wide laser mesa with a 4-μm aperture. Inset shows spectra for pulsed and CW.

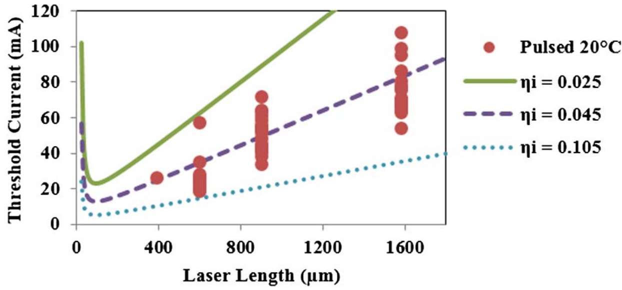

Fig. 5. 20°C pulsed threshold current data for 12-μm mesas with 4-μm-wide current apertures 300°C O_2 plasma assisted bonded to 5 μm of SiO_2 on Si.

$$\frac{1}{\eta_d} = \frac{\alpha_i}{\eta_i \ln(1/R)} L + \frac{1}{\eta_i}. \quad (1)$$

The internal quantum efficiency, η_i, was calculated to be 4.5% from the cutback analysis shown in Fig. 6. This 4.5% curve is plotted with higher and lower bounds of the experimental data in Fig. 5 assuming internal loss, α_i, of 6.2 cm^{-1} and facet reflectivity $R = 0.32$. This performance may be partially owed to poor IV characteristics. These devices suffer from high p-contact resistivity (>13Ω · mm at 200 mA in 4 μm × 2.4 mm laser shown) and turn-on voltage (>2 V) both believed to be due to residual InGaP between the p-GaAs and p-metal. Additional material degradation may be caused by the oxidation anneal evidenced by a decrease in the measured PL

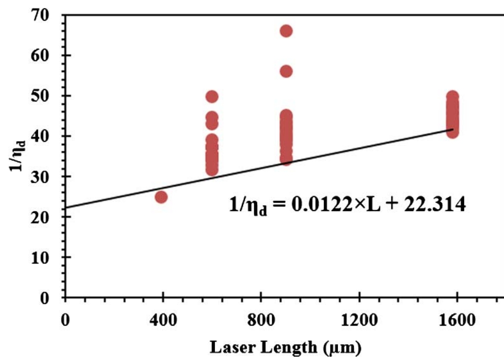

Fig. 6. $1/\eta_d$ plotted versus laser length with a linear fit to best devices of each length to extract internal parameters.

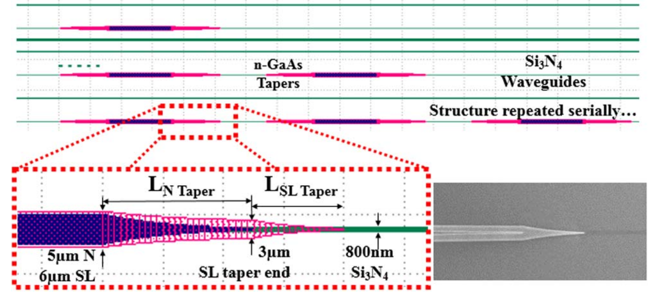

Fig. 7. Schematic of serial tapered n-GaAs to Si_3N_4 loss test structures of two level tapers. III–V is on top of Si_3N_4 waveguides. Inset: SEM of taper prior to top cladding.

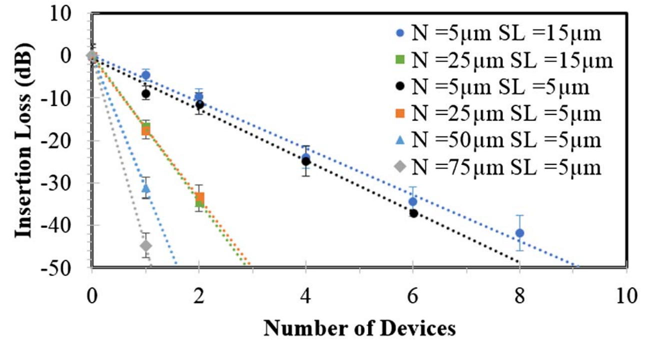

Fig. 8. Transmission loss through tapers of different length. Splits were made for N taper length and SL length as labeled in the legend.

intensity of bonded material before and after this anneal step.

To integrate the III/V-based lasers or amplifiers with passive Si_3N_4 waveguide circuitry, the optical mode has to be coupled from the lower index Si_3N_4 waveguide to the higher index III/V mode, as shown in Fig. 3. Simulation suggested that two adiabatic tapers should be used for this purpose, rather than a single n taper used in the hybrid silicon laser technology [12]. However, due to the higher index contrast between Si_3N_4 and III/V modes, the tips have to be sharper to avoid large losses due to reflections and higher order mode excitation [13]. Sharper tips also tighten the alignment tolerance, so we moved from an i-line stepper to an ASML DUV stepper and have achieved ∼ < 50 nm alignment error. Figure 8 shows some transmission loss measurement data for tapered test structures to quantify the loss of designs with various length of SL and N taper as defined in Fig. 7.

Table 2 details the layers shown in Fig. 7, which represent the n layers of an InGaAs/GaAsP MQW laser epitaxy. The blue layers are the n taper consisting of a sacrificial layer on top of the n contact which acts as a selective etch stop layer to provide a smooth surface for the III–V taper structure rather than a rougher dry-etched surface. Similarly, an additional InGaP layer is used to stop another selective etch above the bonding superlattice (SL). This SL taper is the pink layer that squeezes the mode to and from the green Si_3N_4 waveguide shown in Fig. 6. Each of these two taper layers has an exponential shape down to a ∼150 nm tip, as shown in the inset. Every straight III–V segment is 100 μm.

Table 2. Tapered Test Structure Layers

Taper	Layer	Material	t (nm)	Index (1030 nm)
N	Sacrificial layer	InGaP	50	3.215
N	Contact layer	GaAs	250	3.503
—	Taper interface	—	—	—
SL	SL etch stop	InGaP	20	3.215
SL	Bonding SL	InGaAs/GaAsP	62	3.503

Transmission measurements of test structures with 1, 2, 4, 6, and 8 of these structures were made with TE polarized light from a super luminescent light-emitting diode (SLED) centered on 1045 nm and normalized to transmission through an adjacent straight Si_3N_4 waveguide without any tapered structure. As expected a strong correlation is observed with an increase in the number of serial tapered devices as shown in Fig. 8. The correlation, plotted Fig. 9, shows tapered test structures rapidly increase in insertion loss with longer N tapers, making it unfeasible to even measure repeated structures in the cases with N taper lengths of 50 and 75 µm.

Additional structures with different lengths of straight III–V sections were tested to measure the propagation loss of this segment and remove it from the insertion loss to yield a loss of each taper plotted in Fig. 8. This propagation loss was found to be 44.5 dB/cm. The lowest taper loss of 2.5 ± 0.75 dB was found for tapers with 15-µm SL tapers and 5-µm N tapers with similar result for 5-µm SL tapers of the same N taper length.

These two demonstrations are a significant step toward heterogeneously integrated III–V devices with Si_3N_4 waveguides by means of low temperature bonding. Device performance will need to be improved by a combination of process improvements to improve electrical performance and design improvements to the tapers. Integrating III–V directly onto SiO_2-clad Si_3N_4 shows promise for applications requiring low-loss passive elements for wavelengths shorter than transmittable in circuits using silicon waveguides, such as the hybrid silicon platform [2], while still using the silicon fabrication processes and facilities that make this platform appealing. III–V to Si_3N_4 taper transmission data also suggest that additional tapered mode converter development focus on shorter designs and/or vary parameters such as the gap between the Si_3N_4 waveguide and the bonding interface, epitaxial layer design, and taper shape.

A novel heterogeneous III–V laser integration with broad spectral bandwidth, low-loss passive waveguides, and lower thermal drift Si_3N_4 is proposed with demonstrations toward a new integration platform for back-end CMOS fabrication facilities. CW laser operation of InGaAs/GaAsP MQW lasers is presented with an oxidized current aperture formed on bonded epitaxial material for the first time, to the best of the authors' knowledge. Additionally, taper loss data shows that short tapers have superior performance to longer adiabatic designs.

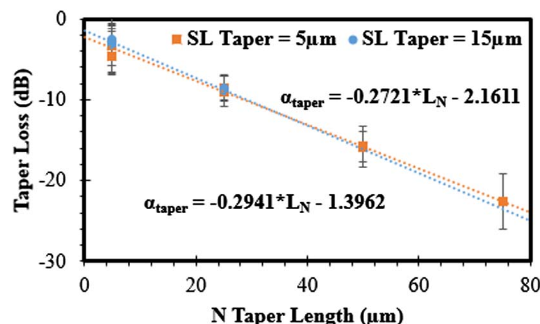

Fig. 9. Taper loss, α_{taper}, extracted from serially repeating structures versus length of N taper, L_N.

Acknowledgements are owed to Peter Craig of ONR and Jinendra Ranka of DARPA/STO for funding this work, UCSB nanofabrication staff, Alexander Fang, Yan Zheng and Chin-Han Lin for helpful discussions.

References

1. H. Park, M. Sysak, H. Chen, A. W. Fang, D. Liang, L. Liao, B. R. Koch, J. Bovington, Y. Tang, K. Wong, M. Jacob-Mitos, R. Jones, and J. E. Bowers, IEEE J. Sel. Top. Quantum Electron. **17**, 671 (2011).
2. M. J. R. Heck, J. F. Bauters, M. L. Davenport, J. K. Doylend, S. Jain, G. Kurczveil, S. Srinivasan, and J. E. Bowers, IEEE J. Sel. Top. Quantum Electron. **19**, 6100117 (2013).
3. B. R. Koch, E. J. Norberg, B. Kim, J. Hutchinson, J.-H. Shin, G. Fish, and A. Fang, in *Optical Fiber Communication Conference/National Fiber Optic Engineers Conference* (Optical Society of America, 2013), paper PDP5C.8.
4. B. Sumpf and K.-H. Hasler, Proc. SPIE **7230**, 72301E (2009).
5. P. Dupriez, A. Piper, A. Malinowski, J. K. Sahu, M. Ibsen, B. C. Thomsen, Y. Jeong, L. M. B. Hickey, M. N. Zervas, J. Nilsson, and D. J. Richardson, IEEE Photon. Technol. Lett. **18**, 1013 (2006).
6. R. Soref, Nat. Photonics **4**, 495 (2010).
7. J. F. Bauters, M. J. R. Heck, D. D. John, J. S. Barton, C. M. Bruinink, A. Leinse, R. G. Heideman, D. J. Blumenthal, and J. E. Bowers, Opt. Express **19**, 24090 (2011).
8. D. Liang and J. E. Bowers, J. Vac. Sci. Technol. B **26**, 1560 (2008).
9. A. Phillips, R. Penty, and I. White, IEE Proc.: Optoelectron. **152**, 174 (2005).
10. M. N. Sysak, H. Park, A. W. Fang, J. E. Bowers, R. Jones, O. Cohen, O. Raday, and M. J. Paniccia, Opt. Express **15**, 15041 (2007).
11. L. Coldren, S. Corzine, and M. Mashanovitch, *Diode Lasers and Photonic Integrated Circuits* (Wiley, 2012).
12. G. Kurczveil, P. Pintus, M. J. R. Heck, J. D. Peters, and J. E. Bowers, IEEE Photon. J. **5**, 6600410 (2013).
13. M. Piels, J. F. Bauters, M. L. Davenport, M. J. R. Heck, and J. E. Bowers, J. Lightwave Technol. **32**, 817 (2014).